SelenIRIS: a Moon-Earth Optical Communication Terminal for CubeSats

1st Jorge Rosano Nonay
Inst. of Communications and Navigation
German Aerospace Center (DLR)
Weßling, Germany
Jorge.RosanoNonay@dlr.de

2nd Christian Fuchs
Inst. of Communications and Navigation
German Aerospace Center (DLR)
Weßling, Germany
Christian.Fuchs@dlr.de

3rd Davide Orsucci
Inst. of Communications and Navigation
German Aerospace Center (DLR)
Weßling, Germany
Davide.Orsucci@dlr.de

4th Christopher Schmidt
Inst. of Communications and Navigation
German Aerospace Center (DLR)
Weßling, Germany
Christopher.Schmidt@dlr.de

5th Dirk Giggenbach
Inst. of Communications and Navigation
German Aerospace Center (DLR)
Weßling, Germany
Dirk.Giggenbach@dlr.de

***Abstract*—Satellite miniaturization and sinking costs of manufacturing and launches are bringing Moon missions in the focus of many space companies and agencies. However, achieving the desired data rates on CubeSats over long ranges is proving increasingly challenging with traditional radio-frequency communication systems. Free-space optical (FSO) communications offer a compact, light, and low-power alternative with higher data throughput and fewer limitations (e.g., fewer governmental regulations, channel interference, eavesdropping...). Based on its long heritage of laser communications and new-space technology, the German Aerospace Center (DLR) is investigating SelenIRIS—a miniaturized terminal for Moon-Earth optical data transmissions—for its OSIRIS program. This paper will analyze the necessary adaptations that are required to transfer the technology from the flight-proven low Earth orbit terminals like OSIRIS4CubeSat (O4C) [1] to a concept mission in Lunar orbit.**

***Index Terms*—OSIRIS, free-space optics, CubeSat, Moon, laser communication, high data rate, new space**

I. Introduction

The space industry is currently experiencing a shift from large individual spacecraft, towards fleets of small-sized CubeSats. This trend is already taking place on Earth orbit and is expected to take over also on other celestial bodies. The main reasons for this shift are technological miniaturization, ampler availability of commercial off-the-shelf (COTS) components, shrinking development and launch costs, shorter development times, standardization, high production scalability, and large area or even worldwide accessibility.

Simultaneously, the data volume and bandwidth requirements are undergoing unprecedented growth. Low-latency transfer of information between a rocketing amount of systems demands ever-increasing data rates, and classical radio frequency (RF) channels are becoming obsolete at the highest exchange rates. Free-space optical (FSO) technology for space applications has finally matured enough to supply the demand generated by the increasing number of satellites and data volume. Besides higher bandwidth capacities, FSO links also present fewer to no mandatory regulations. These, in contrast, limit the available frequency channels in RF communication. Optical systems satisfy lower size, weight, and power (SWaP) requirements than their RF counterparts at the same data rate, making it possible to achieve a data throughput in the order of Gbps even for the smallest terminals [1].

The Institute of Communications and Navigation of the German Aerospace Center (DLR-IKN) has a long heritage of developing laser communication terminals for small satellites in low Earth orbit (LEO). The optical terminal OSIRIS4CubeSat (O4C), its newest development of the Optical Space Infrared Downlink System (OSIRIS) program, provides data rates up to 100 Mbps for direct-to-Earth (DTE) links [1]. Based on its modular technology, OCS wants to develop SelenIRIS, an optical payload on a Lunar orbit that extends its functionalities with sufficient power for a Lunar DTE link. This terminal should help accommodate the necessities of a rapidly expanding market of small satellites on the Moon; e.g., NASA plans to place ten CubeSats on Lunar orbit as part of their Artemis 1 mission, some of which have been developed by ESA and JAXA [2]. These and future spacecraft would profit from FSO communications due to their higher bandwidth, efficiency, compactness, and lower channel crosstalk and regulations over RF systems.

Based on a link budget analysis, this paper describes the necessary technical adaptations to O4C for SelenIRIS. It also presents possible Lunar mission architectures and their radiation environment. We then propose three different concepts for the optical terminal with varying size, weight, and power (SWaP) requirements.

II. State of the Art

DLR's OSIRIS program has a long heritage of flight-proven optical communication terminals for small satellites in LEO. OSIRISv1 and OSIRISv2 explored body pointing mechanisms at data rates up to 1 Gbps. OSIRIS4CubeSat (O4C), seen in

978-1-6654-3439-3/22/$31.00 ©2022 IEEE

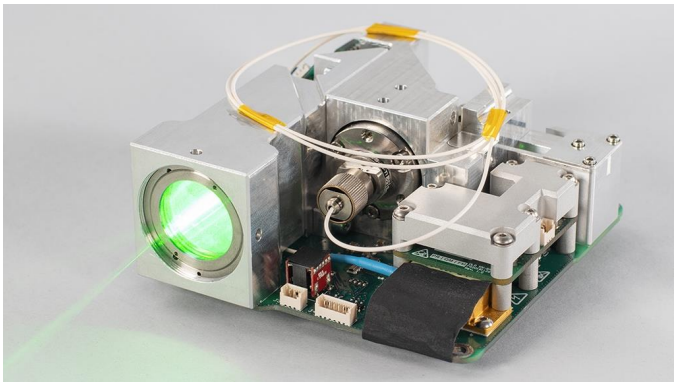

Fig. 1. OSIRIS4CubeSat flight model.

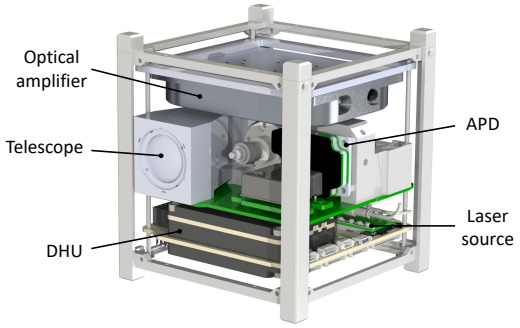

Fig. 2. CubeISL payload concept.

Fig. 1, was launched in 2021 and is the world's smallest optical terminal in space. With a SWaP of 1/3 unit (U), 0.4 kg, and 8.5 W, it transmits data to an optical ground station (OGS) at speeds of 100 Mbps. Its newest development, CubeISL, aims to extend the DTE capabilities of O4C with bidirectional optical inter-satellite links (ISL) [1].

A. *OSIRIS4CubeSat*

O4C is the basis for all OSIRIS missions that follow a miniaturization trend. The compact terminal, shown in Fig. 1, is capable of sending 100 Mbps downlinks to a terrestrial OGS. Its fine pointing assembly (FPA) improved the pointing accuracy compared to past missions. Besides its compactness, its main improvement is the implementation of a 4-quadrant diode (4QD) and a fast steering mirror (FSM) to measure the angular deviation of the beacon laser and align the incoming signal beam with the emitted path [1]. O4C's modular design and use of COTS components allow easy exchange and extension of its subsystems for new missions like CubeISL or SelenIRIS.

B. *CubeISL*

CubeISL is designed to achieve DTE links at 1 Gbps and ISL communications at 100 Mbps. It is expected to fly in 2023. As depicted in Fig. 2, the system has been extended with an optical amplifier that achieves a higher optical output of 1 W to counteract the increased distances of ISL. It incorporates a powerful COTS data handling unit (DHU) to process the higher data rates. The system requires a SWaP of 1 U, 1 kg, and 35 W to allocate its new components [1].

Contrary to O4C, CubeISL will emit and receive high data rates simultaneously. For this purpose, it includes a more sensitive avalanche photodiode (APD) detector besides the 4QD used for tracking. Fig. 3 shows the schematics of the optical terminal. The emitted beam is depicted with red arrows, while the received beam is shown with blue arrows.

III. Mission Architecture

DLR's optical communication payload SelenIRIS primary goal is to demonstrate a Moon-Earth high-speed data link between a CubeSat and an OGS using laser technology. The

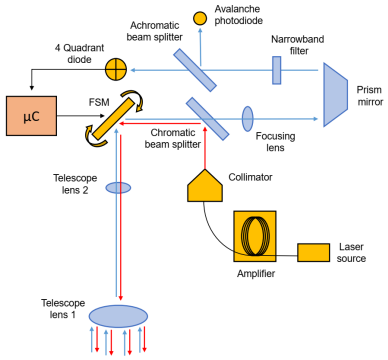

Fig. 3. Diagram of the CubeISL optical terminal.

communication payload would fly on a 6 to 12 U CubeSat, out of which 2 to 6 U should be available for SelenIRIS. The terminal will be designed for a one-year mission duration in Lunar orbit. As a mission requirement, the optical transmission between the payload and the OGS should maintain a reliable link four times a day for ten consecutive minutes. Table I shows a summary of relevant operational parameters for the communication link.

TABLE I
PARAMETERS OF THE SELENIRIS OPTICAL COMMUNICATION LINK

Parameter	Description	Value
Range	Link distance	363 200 - 405 400 km
Wavelength	Downlink	1565 nm
	Uplink	1540 nm
Modulation Scheme	Downlink	NRZ-OOK or PPM
	Uplink	NRZ-OOK or PPM
Coding Scheme	Downlink	RS(255,223) or LDPC ½
	Uplink	RS(255,223) or LDPC ½
Coarse pointing	By the CubeSat	0.1 deg
Fine pointing	By SelenIRIS	µrad-range

The one-year mission time frame does not consider the transfer time from Earth into Lunar orbit. Thus it must be accounted for separately. For this study, we will consider two types of Lunar transfer options: direct and low-thrust transfers.

Direct transfers, as shown in Fig. 4, require high-thrust

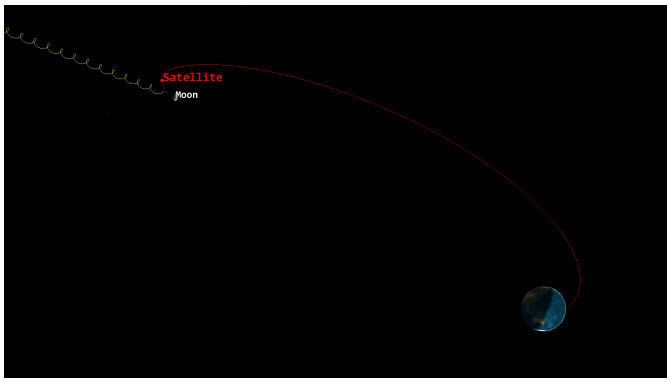

Fig. 4. Direct transfer (red) and insertion into Lunar orbit (yellow).

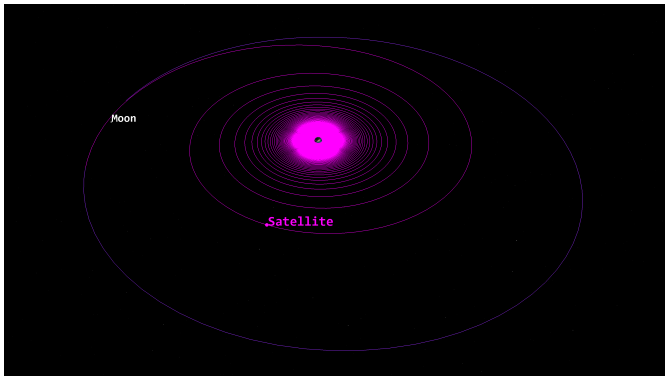

Fig. 5. Low-thrust maneuver from GTO to Lunar orbit.

chemical propulsion systems and large quantities of fuel. Despite being the least fuel-efficient option, they can take as short as a day to place the satellite in a Lunar orbit. With one single pass through the highly energetic Van Allen belts (VAB), this transfer would significantly reduce the payload's required radiation shielding, as will be shown in Subsection IV-A. Typically, a ΔV of 3.9 km/s is required for the trans-Lunar injection from LEO and Lunar-orbit injection [3]. If the trans-lunar injection starts from a geostationary transfer orbit (GTO), the total ΔV shrinks to a minimum of 1.4 km/s [4]. Most launchers are capable of placing a single CubeSat via a direct transfer in Lunar orbit. Heavy-lift vehicles (e.g., NASA's SLS or SpaceX's Falcon heavy) can offer ride-share opportunities for multiple CubeSats [2].

Compact and highly-efficient thrusters can also be used for Lunar transfers and capture in so-called low-thrust maneuvers. Such propulsion systems take advantage of very high specific impulses to decrease total fuel consumption significantly. The total duration can extend from less than a year to several years [4]. Fig. 5 depicts a low-thrust transfer from GTO and its large number of passes through the VAB.

Low-energy maneuvers with a deep-space cruising phase are also a common type of Lunar transfer. They usually require a longer time than direct transfers and more fuel than low-thrust transfers [4]. Hence, this study will focus only on the other two transfer options.

For this study, we have selected three scenarios: a direct transfer from Kennedy Space Center (KSC) spanning over 5 days, a low-thrust maneuver from a 500 km LEO extending for 365 days, and a low-thrust maneuver from GTO for the same length. A final $\sim$2.2-hour Lunar orbit at an altitude of 250 km and 90º inclination was chosen for all three scenarios. The orbital data has been modeled with the Systems Tool Kit (STK) software.

IV. SelenIRIS

SelenIRIS will encounter unprecedented challenges in the OSIRIS program. It must reliably exchange data at a range of 400 000 km, while Earth's turbulent atmosphere randomly distorts its optical beam. The mission will make use of larger mirrors and transmitter power at the OGS, a bigger telescope on the satellite, and more sensitive detection technologies than O4C or CubeISL. Some of the components that will make a link possible are also those most susceptible to damage by high-energy radiative particles. Shielding these components from higher radiation doses than any of the previous OSIRIS missions will be of critical importance.

The following subsections will analyze the radiative space environment and power budget of the SelenIRIS mission. Based on the results, we propose three design concepts with varying SWaP requirements.

A. Radiation Dose

As a consequence of the new-space approach in OSIRIS, its projects rely on COTS components to shrink costs and development time. In most cases, these parts do not have any space heritage. Enduring the harsh environment of space has proven to be one of the biggest challenges for these components. Understanding the conditions that the satellite will encounter is critical to accurately test all sensitive components in advance. Hence, orbital data for each of the three proposed lunar transfer scenarios in Section III—a direct transfer and low-thrust maneuvers from LEO and GTO—has been computed using STK. The radiation dose was simulated with OMERE. Fig. 6 shows a plot with the total cumulative dose for each of the three transfers, including an additional stay of one year around a 2.2-hour lunar orbit.

Radiation levels in Fig. 6 are given as total dose in rad units for varying aluminum shielding thicknesses. These results are summarized in Table II for Al shieldings of 5 and 10 mm. The total cumulative dose was determined with the SHIELDOSE 2 calculator for a silicon solid sphere. It comprises the dose from trapped electrons, trapped protons, solar protons, and secondary photons. Trapped protons and electrons are mainly found spiraling around the inner and outer VAB, respectively. Trapped radiation was simulated for a mission starting in 2024 coinciding with solar maxima conditions, and using the AE8 and AP8 models for electrons and protons. The IGRF magnetic field model was used to portray the effect of the VAB and its particles.

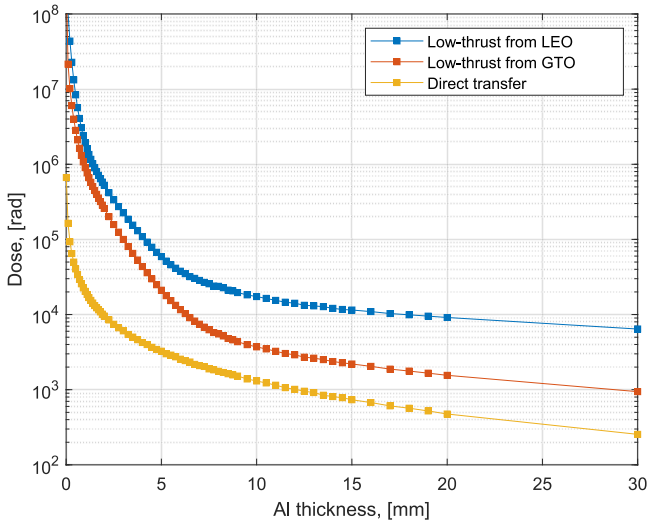

Fig. 6. Total radiation dose for relevant lunar transfers with an additional one-year stay on a 2.2-hour Lunar orbit.

Solar radiation describes any untrapped particle emitted by the Sun. The radiative dose from protons was determined with the ESP model at a confidence level of 97% and from other ions with the Psychic model. The environment of the magnetosphere was calculated with the Störmer magnetospheric cutoff theory.

Secondary photons stem from collisions of high-energetic particles (e.g., cosmic rays) with matter, primarily in the upper atmosphere. Secondary radiation, simulated with the GCR ISO 15390 model, can contribute significantly to the displacement damage and thus should not be neglected [5].

The total dose from Fig. 6 and Table II shows that the received radiation during direct transfers can be neglected due to a singular pass through the VAB and its short time. In this case, we can consider the total dose to be that of the stay around the Lunar orbit. Low-thrust maneuvers from GTO with a one-year stay on the Moon encounter doses on average an order of magnitude higher than for direct transfers. When the trajectory starts from LEO, the satellite will receive on average a radiation dose one order of magnitude higher than from GTO. A duration of one year was chosen for the transfers and orbits due to its simple scalability. New radiation doses can be computed from this value by applying a linear rescaling factor proportional to the actual mission duration.

The most sensitive components on SelenIRIS to radiation damage are the seed laser, the erbium-doped fiber amplifier (EDFA), and the APD detector. Seed laser irradiation with 100 krad(Si) has shown no noticeable deterioration [6], [7]. On the other hand, radiation-induced attenuation (RIA) through point defects can lead to considerable losses on EDFAs. Tests with EDF amplifiers without pumping at 25 krad(Si) showed low degradation of 1 dB/m for the pumped power and 0.5 dB/m for the signal power [8]. The RIA decreases for pumped amplifiers as continuous photo-annealing and recovery take place [9]. Hence, pumping the EDFA would reduce radiation damage

TABLE II
RADIATION DOSE FOR LUNAR TRANSFERS AND ORBITS BY SOURCE

Param.	**Unit**	**Direct transfer**		**Low-thrust (LEO)**		**Low-thrust (GTO)**		**Lunar orbit**	
Time	days	∼5		365		365		365	
Shielding	mm	5	10	5	10	5	10	5	10
Trapped electrons	krad	0.0	0.0	24.0	0.1	12.4	0.0	0.0	0.0
Trapped protons	krad	0.0	0.0	28.7	14.4	1.9	0.9	0.0	0.0
Solar protons	krad	0.1	0.0	1.3	0.5	2.8	1.1	3.2	1.3
Sec. photons	krad	0.0	0.0	1.8	1.0	0.6	0.4	0.0	0.0
Total dose	krad	0.1	0.0	55.7	16.0	17.9	2.4	3.2	1.3

during critical moments while crossing the VAB. Additional tests with even larger radiation doses of 50 krad(Si) showed little degradation of 0.24 dB/m for the input signal. This value could be further lowered to 0.17 dB/m by adding dopants like cerium or hydrogen [10].

APD detectors are the most vulnerable elements to radiation degradation due to increased surface and bulk dark currents. When unbiased, APDs can resist large photon irradiations of 200 krad(Si) [11]. For biased APDs, tests with photon irradiation showed only a fraction of the degradation that occurred for tests with proton irradiation [12]. This difference is due to the high ionization effect of photons versus the typical displacement damage that energetic particles like protons cause, which is the main contributor to the performance decrease of these detectors. The APD's dark current increases linearly with the dose and can lead to deteriorations of up to a few microamperes for extreme radiation conditions of 300 krad(Si) [12]. Radiation testing on relevant detectors for SelenIRIS will be critical to determine the material thickness shielding that will be required for these components.

By limiting the maximum radiation level to 25 krad(Si) for the whole mission duration we ensure that the most critical components do not suffer extensive damage. For direct transfers, this could be achieved with an Al shielding thickness of 1 mm. For low thrust transfers, 5 mm would be needed when starting from GTO and 8 mm for LEO.

B. Optical Link Budget

The design of the communication terminal strongly depends on the results from the link budget. Preliminary power link budgets, with the link budget tool QCalc [13], have shown that to achieve a positive link margin, the OGS would need to be on the order of 80 cm in diameter and emit 60 W of power, and the satellite should have a telescope of 8 cm and 1 W laser power. Moreover, the effect of the atmosphere must also be considered, as it will distort the beam's shape, path, and intensity. Forward error correction (FEC) schemes can be implemented to improve the signal-to-noise ratio of the data exchange. The following sections will discuss these topics in further detail.

Link design:

The system uses spectral isolation to differentiate the emitted and received signals. As in past OSIRIS missions, the wavelengths will also be among the C and L-band (1530 - 1620 nm). For this study, we will use 1540 nm for uplinks and 1565 nm for downlinks. The main reason is the greater availability of COTS high-power emitters at the C-band.

The modulation scheme can be switched between non-return-to-zero (NRZ) on-off keying (OOK) and pulse-position modulation (PPM) to meet the power and bandwidth requirements in different scenarios.

Forward error correction (FEC) codes further improve the link performance by adding redundant parity bits to the transmitted information bits. The receiver's decoder checks them to detect or correct a limited number of bit errors, thus reducing the power requirements and increasing the link margin [14]. For this mission, we will consider Reed-Solomon (RS) and Low-Density Parity-Check (LDPC) encoding, due to their low complexity and high performance, respectively. Convolutional, concatenated, turbo, and fountain codes are not considered due to their higher complexity or lower performance than RS or LDPC codes.

Reed-Solomon (RS) codes with hard decision decoding are often chosen for short to medium-sized blocks due to their low complexity, fast decoding, high data rates, and the absence of error floors. These advantages come at the expense of a moderate coding gain—typically ranging between a few and 5 dB at a BER of 10^{-6}—as compared to an uncoded scheme. OSIRIS missions have previously used an RS(255,223) coding scheme with an overhead of 12.5%. It is widely available on COTS FPGAs and counts with a long heritage on the OSIRIS project. With an RS(255,223) scheme, the BER could be improved from 10^{-3} to about 10^{-6}. In this case, the coding gain (i.e., the decrease in SNR required to achieve the same BER) for a BER of 10^{-6} can be approximated to 4 dB [14].

Low-Density Parity-Check (LDPC) codes offer performances close to the capacity limit at very high data rates. For a similar code rate, LDPC achieves a BER of 10^{-6} with an SNR 3.5 dB lower than an RS scheme. If LDPC with a code rate of 1/2 can be successfully implemented, the link should expect a higher coding gain of 8.5 dB [14].

An interleaving scheme on top of the FEC code can also prevent the loss of whole codewords in the presence of burst errors at the cost of an added delay and memory storage.

Transmitter:

During downlinks, the satellite has to generate an output power of 1 W. Since COTS high-power laser sources do not achieve such high power, the satellite's signal from the seed laser must be boosted with an erbium-doped fiber amplifier (EDFA).

In the case of uplinks, if the OGS were to emit a signal using its large aperture, the beam's divergence angle would be significantly smaller than the deflection angle by which the center of the beam gets displaced while crossing the atmosphere (e.g., beam wander). This scenario would make difficult the tracking procedure and perhaps render it impossible. By emitting four independent beam spots, each with a diameter significantly smaller than the aperture, their divergence angle would exceed the atmospheric beam wander. The divergence becomes 51.9 μrad for a spot size of 4 cm, as compared to the 10.0 μrad beam wander. The antenna gain G_t can be computed as:

$$G_t = \frac{4\pi A_t}{\lambda^2} \cdot \frac{1}{[M^2]^2} \cdot g_t(\alpha, \beta, \gamma, X) \tag{1}$$

where A_t is the effective telescope area, λ is the wavelength, M^2 is a factor of the beam quality, and $g_t(\alpha, \beta, \gamma, X)$ is a transmitter efficiency factor as a function of the truncation factor α, the far-field factor β, the obscuration ratio γ, and the off-axis factor X [15]. In the limit $\alpha \gg 1$, $\beta = 0$, $\gamma = 0$, and $X = 0$, the formula reduces to the gain for an untruncated Gaussian beam. For the OGS, the transmitter efficiency factor is now assumed to be given by $g_t(\sqrt{2}, 0, 0, 0) = 0.748$ and $M^2 = 1.1$. In this new configuration, the OGS transmitter gain decreases from 119.9 dB (for an 80 cm aperture) to 102.1 dB (with four 4 cm beams each having an effective area of $A_t = 12.6$ cm^2). The system thus needs to generate an output power of 60 W or 17.8 dBW to compensate for the losses of the new gain. Multiple manufacturers offer COTS EDFAs with an output between 20 and 30 W. One could achieve the desired output power by combining multiple amplifiers.

The loss from the transmittance of the optical components has been determined based on the design of CubeISL. The transmitter has a transmission factor of 0.94 corresponding to an optical loss of -0.27 dB. The receiver path, which uses more elements, has a transmission of 0.71 and a loss of -1.52 dB.

Deviations in the pointing of the emitter from the ideal line of sight lead to further losses as the receiving terminal does not collect the highest intensity from the Gaussian distributed beam. Assessing the pointing losses with high accuracy requires a mature concept and, in most cases, existing hardware that can be tested. To overcome this issue, we will assume a fixed pointing loss $\eta_p(\phi)$ of -2.0 dB. Based on this value and neglecting bias error and jitter, it is possible to determine the highest allowable pointing error angle ϕ with:

$$\eta_p(\phi) = \left[\frac{\int_\gamma^1 e^{-\alpha^2 u^2} J_0\left(\pi \frac{D_t}{\lambda} \phi u\right) du}{\int_\gamma^1 e^{-\alpha^2 u^2} du} \right]^2 \tag{2}$$

where $J_0(x)$ is the order zero Bessel function of x, and D_t is the transmit aperture diameter [16]. The maximum pointing error during uplinks is 19.9 μrad and 9.0 μrad for downlinks. Adaptive optics can potentially correct the beam wander. But if left uncorrected, the pointing error in uplinks will consist of the atmospheric beam wander (i.e., 10 μrad) and the angular deviation due to the misalignment of the OGS. The maximum allowable angular misalignment of the OGS, in this case,

becomes 9.9 µrad and must be kept below this value to avoid larger pointing losses than -2.0 dB.

Atmospheric Channel:

The biggest challenge for the SelenIRIS mission is overcoming the high losses from the Moon-Earth link distance. The range loss $L_R = [\lambda/(4\pi L)]^2$ [17] varies between -309.5 and -310.4 dB for the Moon's perigee (at 363 200 km) and apogee (at 405 400 km), respectively. On average, we will assume a link distance between the satellite and OGS of 387 500 km and a loss of -310.0 dB.

Additionally, the beam will suffer deflections, shape deformations, attenuation, and intensity fluctuations as it passes over turbulent patches of air. Transmittivity coefficients have been computed with MODTRAN at relevant altitudes. The remaining heights were evaluated via linear interpolation. Since the OGS is located in Weßling (Germany) at 600 m altitude, we computed a mid-latitude summer atmospheric model with a visibility of 23 km and rural aerosol levels. The atmospheric transmission, which follows Beer's law, yields a transmission loss of -0.8 dB in uplinks and -0.5 dB in downlinks at an elevation angle of 30º.

Modeling turbulence in the atmosphere is not an easy task and requires simplifications and approximations. In this study, the refractive index structure parameter $C_n^2(h)$ was computed using the Hufnagel Valley (HV) turbulence profile model:

$$C_n^2(h) = 0.00594 \left(\frac{v}{27}\right)^2 \left(10^{-5}\ h\right)^{10}\ e^{-h/1000} + 2.7 \cdot 10^{-16}\ e^{-h/1500} + A_0\ e^{-h/100} \tag{3}$$

where h is the height, v is the RMS wind speed at high altitudes, and A_0 defines the turbulence strength at the elevation of the ground station [17]. We considered a scenario for night conditions with $A_0 = 1.7 \cdot 10^{-14}\ m^{-2/3}$ and $v = 21\ m/s$ and another for daytime with $A_0 = 1.0 \cdot 10^{-13}\ m^{-2/3}$ and $v = 30\ m/s$. For this link budget analysis, we will use the night HV model.

From the refractive index structure parameter, it is possible to determine the effects caused by the turbulent air as given by [18]. Fluctuations in the angle-of-arrival (AoA) produced by beam deflections lead to jitter or dancing of the image on the detector plane. During uplinks, the AoA fluctuations account for only 0.2 nrad. Downlinks, on the other hand, will experience deviations of 1.7 µrad. These can be corrected at the OGS via first-order adaptive optics (i.e., tip-tilt mirrors).

Over long-term time frames, the beam's spot size during uplinks expands over a larger area in an effect called beam spreading. Its broadening is approximately proportional to the hard aperture of the transmitter [18]. As the effective aperture of the OGS for uplinks has been reduced to 4 cm, the beam gets expanded by just 2.2% and will not be further considered. However, over short-term periods, the instantaneous center of the beam gets displaced randomly by the beam wander. Same as the beam spreading, beam wander only affects uplinks [18]. For elevation angles of 30º and a reduced hard aperture of 4 cm, the variance of the angular RMS value of the beam wander becomes 10.0 µrad. The angular beam wander is included in the link budget as an additional pointing error.

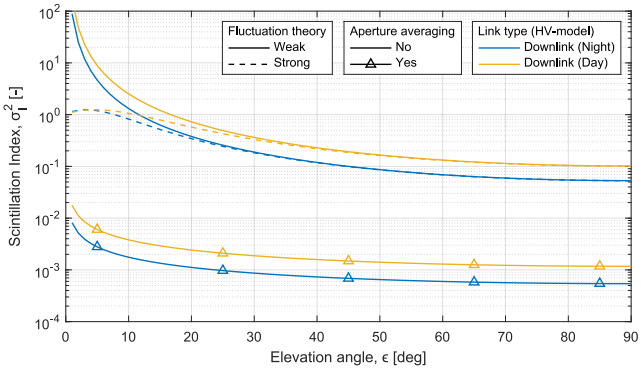

Fig. 7. Effect of aperture averaging on the scintillation index in downlinks.

The scintillation index measures the random intensity variations caused by the turbulent atmosphere. A detailed description of its simulation for different link scenarios and turbulence strengths is out of the scope of this paper and is given by [18]. A multiple-input-single-output (MISO) configuration with identical beams, reduces the scintillation index σ_I^2 by a factor proportional to the number n_b of beams used—$\sigma_{I,MISO}^2 = \sigma_{I,SISO}^2/n_b$ [19]. Additionally, in downlinks, when the telescope aperture is larger than the spatial coherence radius, the non-uniform irradiance gets integrated over the whole collecting aperture in an effect called aperture averaging [17], [18]. As depicted in Fig. 7, aperture averaging leads to a drastic reduction of the scintillation index. The plot compares the decrease in the scintillation index when considering aperture averaging to a point source telescope without aperture averaging. The results are given for a weak and strong fluctuation theory, and day and night HV turbulence models. Point receivers exhibit saturation at low elevation angles, which can only be described using a strong turbulence fluctuation theory. However, the model for aperture averaging using weak fluctuation theory fits well with empirical measurements even at very low elevations [20].

The random intensity variations from scintillation cause, on average, a fading loss. Its fluctuations are described best by a lognormal probability density function, which can be used to determine a new effective bit error rate (BER) [19]. A more general method to describe the fading loss in a turbulent channel uses a threshold probability p_{thr} to determine an effective scintillation loss L_{sci}, and is given by:

$$L_{sci} = 4.343 \left[\mathrm{erf}^{-1}\left(2p_{thr} - 1\right) \sqrt{2\ln\left(\sigma_I^2(D) + 1\right)} - \frac{1}{2}\ln\left(\sigma_I^2(D) + 1\right) \right] \tag{4}$$

where erf^{-1} stands for the inverse error function and $\sigma_I^2(D)$ for the scintillation index averaged over the aperture D [21]. With a scintillation index of 0.033 during uplinks and a

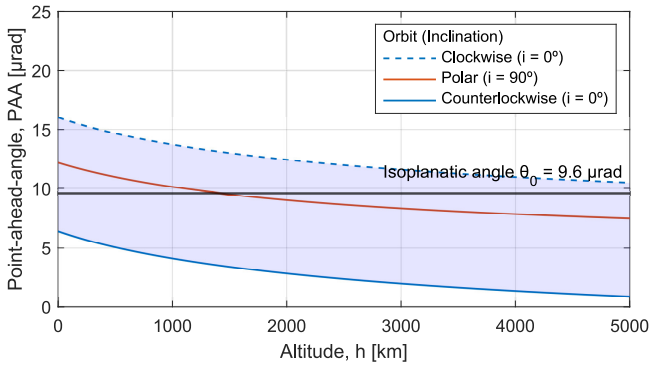

Fig. 8. Point-ahead angle of a satellite over its altitude for three Lunar orbits.

threshold probability of 10^{-3}, the loss due to scintillation becomes -2.5 dB. The scintillation index for downlinks is much smaller due to aperture averaging (i.e., $\sigma_I^2(D) = 0.0008$) and yields a fading loss of just -0.4 dB.

Another critical aspect of FSO communications with satellites is the point-ahead angle (PAA). The emitter's pointing mechanism must compensate for the change in the spacecraft's position during the signal round-trip time due to the spacecraft's high velocity. Whether the path of the uplink channel undergoes the same atmospheric conditions as the downlink channel (i.e., reciprocal channels) depends on whether the isoplanatic angle is larger or smaller than the PAA [18]. The PAA of the satellite on Lunar orbit was determined considering its orbital speed, the Lunar orbital speed around Earth, and the rotational speed of the topocentric OGS. Fig. 8 shows the PAA of a Lunar satellite on three relevant orbits: equatorial clockwise, polar, and equatorial counterclockwise. Shaded in blue are all possible values for the PAA at different inclinations. For comparison, the black line represents the isoplanatic angle for an elevation of 30º of 9.6 μrad. A reciprocal channel for up and downlinks requires that the PAA is smaller than the isoplanatic angle. The advantage of passing both beams through the same patch of the atmosphere lies in the possibility of correcting wavefront distortions with adaptive optics. Alternatively, the OGS would require a synthetic beacon or a laser guide star [18]. Careful selection of the satellite altitude and inclination will influence how distortions can be corrected.

Receiver:

The receiver gain G_r is given analogous to the transmitter gain G_t in (1) by:

$$G_r = \frac{4\pi A_r}{\lambda^2}(1-\gamma^2) \tag{5}$$

where A_r is the area of the receiver's primary mirror, and γ is its obscuration ratio [22]. The gain for uplinks using an 8 cm aperture receiver is 103.7 dB, and for downlinks with an 80 cm receiver, 123.6 dB.

Further losses to consider at the receiver are splitting and coupling losses. The receiver uses two detectors—one for beam tracking and one for data reception—and the incoming signal has to be split between both detectors. For this study, we will use a 50/50 splitting ratio and therefore, a splitting loss of -3 dB for each channel.

After the signal has been forked it must be coupled onto the detector surface or an optical fiber. Its coupling efficiency is strongly dependent on the receiver radius [22]. With a typical core diameter of 9 μm, optical fibers will suffer a coupling loss of -5.0 dB. The losses when coupling onto the detector's surface are almost negligible due to its comparably large size.

Optical Link Budget:

A robust optical link exhibits a link margin of 3 dB between the power at the detector and that required to achieve a specific BER. Using Friis' transmission equation for all the relevant gains and losses, it is possible to determine the power that reaches the detector surface for each channel, as given in Table III for uplinks and Table IV for downlinks. The effective power at the detector results from adding the coding gain to the detector power. The results are given for an OOK-NRZ modulation format, an RS(255,223) FEC coding scheme, night conditions simulated with the HV night model, a satellite elevation of 30º, and an IM/DD detection technology.

TABLE III
UPLINK LINK BUDGET (ALL VALUES ARE GIVEN IN dB)

Parameter		Uplink	
		Comm.	Tracking
Tx	Coding gain	4.0	0.0
	Mean power	17.8	17.8
	Antenna gain	102.1	102.1
	Optical loss	-0.3	-0.3
	Pointing loss	-2.0	-2.0
Ch	Range loss	-310.0	-310.0
	Atmospheric attenuation	-0.8	-0.8
	Scintillation loss	-2.5	-2.5
Rx	Antenna gain	103.7	103.7
	Optical loss	-1.5	-1.5
	Splitting loss	-3.0	-3.0
	Coupling loss	0.0	0.0
LB	Power at detector	-96.5	-96.5
	Effective power	-92.5	-96.5

TABLE IV
DOWNLINK LINK BUDGET (ALL VALUES ARE GIVEN IN dB)

Parameter		Downlink	
		Comm.	Tracking
Tx	Coding gain	4.0	0.0
	Mean power	0.0	0.0
	Antenna gain	99.8	99.8
	Optical loss	-0.3	-0.3
	Pointing loss	-2.0	-2.0
Ch	Range loss	-310.0	-310.0
	Atmospheric attenuation	-0.5	-0.5
	Scintillation loss	-0.4	-0.4
Rx	Antenna gain	123.6	123.6
	Optical loss	-1.5	-1.5
	Splitting loss	-3.0	-3.0
	Coupling loss	-0.1	0.0
LB	Power at detector	-94.4	-94.3
	Effective power	-90.4	-94.3

An experimental analysis of the 4QD detector used for the tracking channel showed that 250 pW or -96.0 dBW of power are needed to achieve accurate tracking. Its link margin is shown in Table V. The low margin proves that the satellite will not reliably track the OGS beacon, especially during uplinks. To improve the tracking channel, a more sensitive detector could be designed with a minimum required sensitivity of 100 pW. Alternatively, one could enlarge the satellite's telescope aperture. A 12 cm primary mirror would increase the link margin in up and downlinks by 3.6 dB at the expense of additional volume requirements. This last option will be further discussed in Subsection IV-C.

TABLE V
LINK MARGIN FOR THE TRACKING CHANNEL

Parameter	Tracking	
	Uplink	Downlink
Effective power	-96.5 dBW	-94.3 dBW
Rx required power	-96.0 dBW	-96.0 dBW
Link margin	-0.5 dB	1.7 dB

As for the communication channel, the required power at the APD detector for a specific BER can be determined with:

$$P_{req} = E_p r_b S \tag{6}$$

where $E_p = (\hbar c)/\lambda$ is the photon's energy, $\hbar$ is Planck's constant, r_b is the system's data rate, and S is the detector's sensitivity for a given BER in photons per bit [17]. By selecting a required power at any detector 3 dB lower than the effective power, we can ensure a link margin of the same magnitude. Considering a state-of-the-art APD with a sensitivity of 500 photons per bit for a BER of 10^{-9} [23], we obtain the necessary data rate r_b to achieve the required power for a reliable link. Table VI gives the resulting data rates for a robust Moon-Earth optical link with the SelenIRIS terminal.

TABLE VI
ACHIEVABLE DATA RATES FOR THE COMMUNICATION CHANNEL

Parameter	Comm.	
	Uplink	Downlink
Effective power	-92.5 dBW	-90.4 dBW
Rx required power	-95.5 dBW	-93.4 dBW
Data rate	4.4 Mbps	7.2 Mbps

Comparison with SOTA RF communication:

Based on the results from the link budget, it has been shown that with the current technological stand, DLR can develop a CubeSat communication terminal for high data rate exchange between a Lunar satellite and a ground station. The current RF standard terminal for Lunar CubeSats is the JPL IRIS v2.1 radio transceiver. At its full transmitting capabilities, the terminal utilizes a SWaP of 0.78 U, 1.3 kg, and 35 W. In connection with the Deep Space Network (DSN), the LunaH-Map CubeSat will achieve a maximum downlink rate of 256 Kbps and uplink rates of 8 Kbps. Using a moderate-sized antenna with a 21 m dish and 10 kW uplink power, the system's data rate decreases to just 8 Kbps for downlinks and 1 Kbps on uplinks [24].

As summarized in Table VI, in its simplest configuration of 2 U, 1.7 kg, and 35 W, SelenIRIS would achieve 4.4 Mbps in uplinks and 7.2 Mbps in downlinks. The downlink rate represents a nearly 30-fold increase compared to the JPL IRIS radio terminal in conjunction with the DSN. An additional advantage of FSO systems over their RF counterparts is the increased availability of small-sized antennas at a significantly lower operating cost.

For the most data-hungry transmissions, the 4 to 6 U configurations incorporate a coherent transceiver. The 6 U concept adds a 12 cm telescope which would allow using the same tracking detector as in past OSIRIS missions. The following subsection describes these concepts in more detail.

It must be noted, that this study has solely focused on APD detection technologies. Better detectors—e.g., superconducting nanowire single-photon detectors (SNSPD)—or larger telescopes can be used at the ground station to improve downlink data rates.

C. Payload Design

The SelenIRIS mission has been designed based on the experience and hardware of O4C and CubeISL. Different concept designs have been proposed to meet varying SWaP requirements. In its elementary configuration of 2 units, as shown in Fig. 9, the system includes a 1 U telescope with an 8 cm aperture and an intensity modulation and direct detection (IM/DD) receiver. 1 U is the most compact telescope volume that can incorporate the large-aperture required from the link budget analysis. The COTS telescope is made of SiC to withstand temperature drifts with minimal deformation and weighs less than 0.7 kg. The collecting aperture has been maximized, resulting in an obscuration ratio of 0.3.

The optical transceiver includes an emitter with a seed laser that receives information and telemetry from the data handling unit (DHU). The laser signal is then amplified to 1 W by the EDFA, passed through a collimator, and exits the terminal through the two-mirror telescope. At the receiver, the signal enters through the telescope and is reflected on the fast-steering mirror (FSM). The FSM accurately aligns the incoming signal path with the center of the 4-quadrant detector (4QD). The reflected beam from the FSM crosses the chromatic beamsplitter, aligning the emitted and received signal along the same path. It is then forked at an achromatic beamsplitter which divides its intensity between the 4QD tracking detector and the more sensitive APD sensor for the data. On the core of the transceiver is a microcontroller in charge of exchanging telemetry with the DHU, processing the data from the tracking sensor, and forwarding information to the FSM actuator.

Placed at the base of the terminal is the DHU. This processing unit handles most of the information, monitors critical components, and communicates with the satellite's onboard computer (OBC). A radiation-hardened COTS FPGA has been

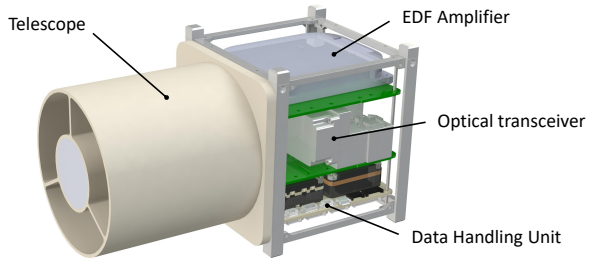

Fig. 9. System design of the 2 unit optical terminal.

chosen with the capability to simultaneously write and read the data of the optical terminal at a maximum speed of 1 Gbps.

Table VII details each concept's expected size, weight, and power (SWaP) requirements. The 2 U design is comprised of a 1 U telescope and a 1 U optical terminal. The telescope weighs 0.7 kg and the transceiver 1 kg. The whole system requires 35 W of power during operation.

TABLE VII
SIZE, WEIGHT, AND POWER ANALYSIS FOR RELEVANT DESIGN CONCEPTS

Volume	Size	Weight	Power
2 units	20x10x10 cm	1.7 kg	35 W
4 units	20x20x10 cm	3.2 kg	58-75 W
6 units	25x15x15 cm	4.0 kg	58-75 W

The 4 U configuration expands the functionality of the 2 U concept with a coherent receiver. To accommodate the increased volume requirement, two additional units have been allocated for this purpose. This configuration shows a trade-off between a larger SWaP (see Table VII) in exchange for enhanced sensitivities of 100-200 ppb for the satellite's coherent receiver. The coherent transceiver weighs around 1.5 kg and consumes an additional 23 to 40 W of power.

The OGS will also need a coherent transceiver. Due to its size—larger than 40 cm—, the coherent signal has to be corrected with adaptive optics (AO) before mixing the received beam with the local oscillator. The coherent detector at the OGS combined with AO requires only 40 ppb to achieve the same BER as an IM/DD APD detector with a sensitivity of 500 ppb. For a sensitivity of 40 ppb and a required power of -93.4 dBW, the achievable data rate for downlinks increases drastically to 90 Mbps. The data rate can be improved even further with single-photon detectors, like SNSPD.

Besides the coherent receiver, in its biggest configuration of 6 U, the satellite also includes a larger telescope of 3.3 U and 12 cm aperture. The telescope's weight increases to 1.5 kg, while its gain improves by 3.6 dB. The communication data rate would increase to 10 Mbps during uplinks and 16 Mbps during downlinks. Moreover, the tracking link margin would improve enough to allow maintaining the same tracking technology as has been used in past OSIRIS missions. However, the ampler aperture leads to a smaller divergence angle during downlinks, thus diminishing the allowable OGS angular pointing error from 9.0 µrad to 6.1 µrad in order to maintain the same pointing loss of -2.0 dB.

V. SUMMARY AND OUTLOOK

In this paper, we present SelenIRIS: a high data rate Moon-Earth optical communication terminal for Lunar CubeSats. We have described three relevant Lunar transfer options for CubeSats and analyzed the environmental radiation dose for each scenario and mission duration. In a worst-case scenario with a slow-thrust maneuver and one-year mission duration, the total radiation dose still meets the acceptable levels tested on most COTS components that were used in previous missions.

A link budget between a Lunar satellite and a terrestrial ground station has assessed the first-order limitations of the optical terminal. It has proven that the current bottleneck lies at the tracking channel and, especially, the 4QD sensitivity. Ensuring that a robust link can be held will need either a component redesign or a larger telescope at the satellite. With these improvements, SelenIRIS would achieve data rates of 4.4 Mbps for uplinks and 7.2 Mbps for downlinks. These rates represent a 550-fold improvement in uplinks and a 28-fold improvement in downlinks compared to SOTA RF terminals with similar SWaP requirements. Additionally, an optical link would significantly reduce requirements and costs for the ground station.

The aforementioned data rates are given for the simplest 2 unit configuration proposed for the SelenIRIS mission. At the expense of additional SWaP requirements, the system can be extended with a 2 U coherent receiver or a 3.3 U telescope with a 12 cm aperture. With a coherent detection scheme, downlink rates of 90 Mbps would be possible, and even faster data rates can be achieved with single-photon detectors. Future studies will discuss these improvement possibilities in more detail.

ACKNOWLEDGMENT

We would like to especially thank Andrea M. Carrillo Flores from the Institute of Communications and Navigation at DLR for her contribution to the link budget analysis under atmospheric turbulence effects and her help in the revision of this paper.

REFERENCES

[1] B. Rödiger, C. Fuchs, J. R. Nonay, W. Jung, and C. Schmidt, "Miniaturized Optical Intersatellite Communication Terminal – CubeISL," 2021 IEEE International Conference on Communications Workshops (ICC Workshops), pp. 1-5, 2021.

[2] D. M. McIntosh, J. D. Baker, and J. A. Matus, "The NASA CubeSat Missions Flying on Artemis-1", NASA/34th Annual Small Satellite Conference, Paper SSC20-WKVII-02, 2020.

[3] J. Parker and R. Anderson, "Low-Energy Lunar Trajectory Design", JPL NASA, 2014.

[4] D. Folta, D. Dichmann, P. Clark, A. Haapala, and K. Howell, "Lunar Cube Transfer Trajectory Options", NASA/AAS Space Flight Mechanics Meeting, Paper AAS 15-353, 2015.

[5] S. Buchner, P. Marshall, S. Kniffin, and K. LaBel, "Proton Test Guideline Development – Lessons Learned", NASA/Goddard Space Flight Center, 2002.

[6] I. Esquivias, and others, "Evaluation of the radiation hardness of GaSb-based laser diodes for space applications", 12th European Conference on RADECS, pp. 349-352, 2011.

[7] P. Henderson, and others, “Space validation of 1550nm DFB laser diode module”, Proc. SPIE 11180, International Conference on Space Optics – ICSO 2018, 111805G, 2019.
[8] A. Ladaci, and others, “Optimized radiation-hardened erbium doped fiber amplifiers for long space missions”, Hournal of Applied Physics 121, 163104, 2017.
[9] J. Ma, and others, “Space radiation effect on EDFA for inter-satellite optical communication”, Optik 121, pp. 535–538, 2008.
[10] T. S. Rose, D. Gunn, and G. C. Valley, “Gamma and proton radiation effects in Erbium-doped fiber amplifiers: Active and passive measurements”, Journal of lightwave technology, Vol. 19, 2001.
[11] A. S. Huntington, L. A. Sellsted, M. A. Compton, and E. W. Taylor, “Mesa-isolated InGaAs avalanche photodiode damage by ionizing radiation”, Proc. SPIE 8164, Nanophotonics and Macrophotonics for Space Environments V, 816404, 2011.
[12] H. N. Becker and A. H. Johnston, “Dark current degradation of near infrared avalanche photodiodes from proton irradiation”, IEEE Transactions on Nuclear Science, vol. 51, no. 6, pp. 3572-3578, 2004.
[13] D. Orsucci, J. R. Nonay, A. Shrestha, and F. Moll, “QCalc: a tool to compute classical and quantum communication rates over free-space optical channels”, Proc. SPIE 11868, Emerging Imaging and Sensing Technologies for Security and Defence VI, 118680F, 2021.
[14] R. Barrios, B. Matuz, and R. Mata-Calvo, “Satellite Communications in the 5G Era: Ultra-high-speed data relay systems”, IET Telecommunications Series, vol. 79, pp. 341-373, 2018.
[15] B. J. Klein and J. J. Degnan, “Optical antenna gain 1: Transmitting antennas”, Applied Optics, vol. 13, pp. 2134-2141, 1974.
[16] W. K. Marshall and B. D. Burk, “Received optical power calculations for optical communications link performance analysis”, NASA/Communications Systems Research Section, TDA Progress Report 42-87, pp. 32-40, 1986.
[17] H. Hemmati, “Near-Earth Laser Communications”, CRC Press, 2009.
[18] L. C. Andrews and R. L. Phillips, “Laser Beam Propagation through Random Media”, SPIE, 2nd Edition, 2005.
[19] A. Mustafa, D. Giggenbach, J. Poliak, and S. T. Brink, “Quantifying the effect of the optimization of an m-fold transmitter diversity scheme with atmospherically induced beam wander and scintillation”, Photonic Networks, vol. pp. 1–3, 2019.
[20] D. Giggenbach and F. Moll, “Scintillation Loss in Optical Low Earth Orbit Data Downlinks with Avalanche Photodiode Receivers”, IEEE International Conference on Space Optical Systems and Applications (ICSOS), pp. 115-122, 2017.
[21] D. Giggenbach and H. Henniger, “Fading-loss assessment in atmospheric free-space optical communication links with on-off keying”, Optical Engineering, vol. 47, pp. 046001 1–6 , 2008.
[22] J. J. Degnan and B. J. Klein, “Optical antenna gain 2: Receiving antennas”, Applied Optics, vol. 13, pp. 2397–2401, 1974.
[23] M. S. Ferraro, and others, “Impact-ionization-engineered avalanche photodiode arrays for free-space optical communication”, Optical Engineering, vol. 55(11), 111609, 2016.
[24] A. Babuscia, C. Hardgrove, K. M. Cheung, P. Scowen, and J. Crowell, “Telecommunication System Design for Interplanetary CubeSat Missions: LunaH-Map”, 2017 IEEE Aerospace Conference, pp. 1-9, 2017.